RESEARCH METHODS

Glyoxal fixation: An approach to solve immunohistochemical problem in neuroscience research

Kohtarou Konno[1], Miwako Yamasaki[1], Taisuke Miyazaki[2], Masahiko Watanabe[1]*

The gold-standard fixative for immunohistochemistry is 4% formaldehyde; however, it limits antibody access to target molecules that are buried within specialized neuronal components, such as ionotropic receptors at the postsynapse and voltage-gated ion channels at the axon initial segment, often requiring additional antigen-exposing techniques to detect their authentic signals. To solve this problem, we used glyoxal, a two-carbon atom di-aldehyde. We found that glyoxal fixation greatly improved antibody penetration and immunoreactivity, uncovering signals for buried molecules by conventional immunohistochemical procedures at light and electron microscopic levels. It also enhanced immunosignals of most other molecules, which are known to be detectable in formaldehyde-fixed sections. Furthermore, we unearthed several specific primary antibodies that were once judged to be unusable in formaldehyde-fixed tissues, allowing us to successfully localize so far controversial synaptic adhesion molecule Neuroligin 1. Thus, glyoxal is a highly effective fixative for immunostaining, and a side-by-side comparison of glyoxal and formaldehyde fixation is recommended for routine immunostaining in neuroscience research.

INTRODUCTION

Before immunohistochemical incubation, tissues and cells must be fixed to prevent decay and loss of biological structure and constituent molecules by autolysis or putrefaction. Formaldehyde is a one-carbon atom mono-aldehyde, and 4% formaldehyde has long been the gold-standard fixative for immunohistochemistry. In laboratories, 4% formaldehyde is prepared by depolymerization of paraformaldehyde (PFA) or 1:10 dilution of saturated (40% w/v) formalin and is, therefore, also referred to as 4% PFA or 10% formalin, respectively. Glutaraldehyde, a five-carbon atom dialdehyde, is added to formaldehyde for ultrastructural preservation in electron microscopy. These aldehydes are classified as cross-linking fixatives, which act by creating covalent chemical bonds between amino groups on proteins and nucleic acids. However, chemical fixation by aldehydes, especially glutaraldehyde, hampers immunoreactions by inducing conformational changes or destruction of epitopes, which lowers the binding affinity of an antibody for an antigen, and also by shrinking tissues, which physically hinder antibody access to the antigen. For these reasons, chemical fixation often diminishes the sensitivity and specificity of immunohistochemical detection. This is particularly problematic in immunostaining for ionotropic receptors, ion channels, and their interacting molecules, which are condensed at specialized neuronal compartments, such as the postsynaptic density, synaptic cleft, and axon initial segment (*1*, *2*).

This problem was first noted by Baude *et al.* (*3*, *4*). They concluded that a postembedding immunogold method is the only reliable method to detect synaptic AMPA-type glutamate receptors (AMPARs), while pre-embedding immunoelectron microscopy, with either immunoperoxidase or immunogold, can efficiently detect extrasynaptic and glial AMPARs. To overcome this problem, we and others have modified formaldehyde-based immunohistochemistry by developing antigen-exposing techniques, such as pepsin digestion before immunohistochemical incubation (*5*) and microwave irradiation during fixation (*6*). Similarly, lowering formaldehyde concentrations and pH for tissue fixation improved detection (*7*). With these techniques, weak diffuse labeling by conventional immunohistochemistry turned into intense labeling of various ionotropic receptors, ion channels, and their scaffold at particular compartments: NMDA-type glutamate receptors (NMDARs) and postsynaptic density protein 95 (PSD-95) (*5*, *6*, *8*) in the neuropil, γ-aminobutyric acid type A ($GABA_A$) receptors ($GABA_A$Rs) (*6*) along the cell surface, and voltage-gated Na_v and K_v channels (*2*, *7*) at the axon initial segment. Nevertheless, appropriate application of these techniques needs more experience, time, and effort than conventional immunohistochemistry, hampering their widespread use in the neuroscience field.

Glyoxal is a two-carbon atom dialdehyde. It has been used to denature nucleic acid strands in Southern and Northern blot analyses (*9*) but rarely for tissue fixation in histological and histochemical analyses (*10*). Recently, Richter *et al.* (*11*) reported glyoxal as an alternative fixative to formaldehyde in immunocytochemistry. They revealed that glyoxal is superior to formaldehyde, with faster cross-linking ability, better preservation of cell morphology, and higher signal intensity for many molecules. In the present study, we tested whether glyoxal fixation could solve the above problem in neuroscience research. Here, we show that specific antigen-exposing techniques are no longer necessary for immunohistochemical detection of various molecules in glyoxal-fixed brain tissues and further demonstrate its versatility in deep imaging, immunoelectron microscopy, paraffin-embedded sections, and rodent's and primate's brains.

[1]Department of Anatomy, Faculty of Medicine, Hokkaido University, Sapporo 060-8638, Japan. [2]Department of Functioning and Disability, Faculty of Health Sciences, Hokkaido University, Sapporo 060-8638, Japan.
*Corresponding author. Email: watamasa@med.hokudai.ac.jp

RESULTS

Protocol optimization

Richter *et al.* (*11*) reported a 3% glyoxal fixative containing 0.8% acetic acid and 20% ethanol as an effective alternative to 4% PFA for immunostaining. To confirm and optimize this fixative for the detection of synaptic molecules, we tested different compositions of glyoxal fixatives and compared them with 4% PFA by measuring the intensity of immunofluorescence signals in particular brain regions of interest or in whole-brain sections of adult mice, unless otherwise noted. For this analysis, we selected four presynaptic molecules (Bassoon, vesicular glutamate transporters VGluT1 and VGluT2, and vesicular inhibitory amino acid transporter VIAAT; fig. S1) as representative molecules that are detectable in formaldehyde-fixed tissues by conventional immunohistochemical methods (*12*, *13*). We also selected four postsynaptic molecules (AMPAR GluA2, $GABA_AR\alpha1$, and scaffolding proteins PSD-95 and gephyrin; Fig. 1A), as those that require antigen-exposing techniques for immunohistochemical detection in formaldehyde-fixed tissue, such as section pretreatment by pepsin or microwave irradiation for light microscopy (*5*, *6*, *8*) and postembedding immunogold for electron microscopy (*4*, *14*).

Compared with 4% PFA (PFA column), signal intensity in the cerebellar cortex was remarkably increased with all four glyoxal fixatives for all four presynaptic molecules (fig. S1) and all four postsynaptic molecules (Fig. 1A). Among the glyoxal fixatives, fixation by 3% glyoxal only (G) or 3% glyoxal/0.8% acetic acid (GAA) stably yielded greater intensification than that by 3% glyoxal/20% ethanol (GE) or 3% glyoxal/0.8% acetic acid/20% ethanol (GAAE) (Fig. 1A and fig. S1). This improvement was quantified by measuring the mean fluorescence intensity in the molecular layer and expressing it as a ratio relative to that obtained with 4% PFA fixation (Fig. 1A and fig. S1). One major disadvantage of glyoxal fixation is that tissue sections are fragile, and the white matter is prone to tear, most typically along the corpus callosum, during immunohistochemical processing. Increasing the concentration of glyoxal up to 9% and adding 8% acetic acid was effective in tissue hardening, preventing section deformity and breakage without compromising signal intensity, as assessed by PSD-95 labeling in the cerebral cortex and striatum (fig. S2).

Use of low concentrations of PFA can enhance immunohistochemical signals for ionotropic glutamate receptors (iGluRs), ion channels, and their scaffold proteins (*7*, *15*, *16*). Therefore, we next compared signal intensity for scaffolding proteins, PSD-95 and synapse-associated protein 102 (SAP-102), in the cerebral cortex and striatum fixed by 4% PFA, 1% PFA, and 9% glyoxal/8% acetic acid (fig. S3). While 1% PFA fixation tended to increase immunofluorescence signals compared with 4% PFA fixation, much stronger and clearer labeling was obtained with fixation by 9% glyoxal/8% acetic acid for both PSD molecules. We further found that the addition of 0.1% Triton X-100 to incubation and washing buffer (PBS-T) was essential to elicit these improved effects by glyoxal fixation. Figure 1 (B to D) shows NMDAR GluN2C labeling at synaptic glomeruli in the cerebellar granular layer. Punctate GluN2C labeling around VGluT1-labeled mossy fiber terminals was visible only when PBS-T, but not phosphate-buffered saline (PBS), was used as an incubation and washing buffer. No such improvement by PBS-T was found for 4% PFA–fixed sections. Similar improvements were observed for VGluT2 and AMPAR labeling in brains of the common marmoset, a small New World primate, by fixation with 9% glyoxal/8% acetic acid and use of PBS-T (Fig. 2).

On the basis of these tests, we concluded that glyoxal has great potential for immunohistochemical detection of synaptic molecules and that fixation by 9% glyoxal/8% acetic acid (hereafter termed GAA fixative) and use of Triton X-100–containing buffer constitute the optimum protocol to be adopted for both rodent and primate brains. We, therefore, tested the utility of this protocol in molecular detection in neuroscience research by comparing GAA fixation with 4% PFA fixation (hereafter PFA fixation) in the adult mouse brain.

No need for antigen-exposing techniques

Among synaptic molecules, NMDAR subunits and their PSD-95 scaffold proteins require strong antigen-exposing techniques for pre-embedding immunohistochemistry with PFA-fixed tissues (*5*, *6*, *8*). Without pepsin pretreatment, signals for NMDAR GluN1 are virtually invisible in PFA-fixed sections (Fig. 3, A to C). In GAA-fixed sections, GluN1 was readily detectable all over the brain, with higher levels in the hippocampus, cerebral cortex, striatum, and cerebellar granular layer (Fig. 3D). The specificity of GluN1 signals in GAA-fixed tissues was supported by blank labeling of GluN1 signals on parvalbumin(+) neurons in the reticular thalamic nucleus of PV-Cre^+; $GluN1^{flox/flox}$ mouse brains (fig. S4). In the hippocampus, GluN1 was particularly enriched in the stratum oriens and radiatum of the CA1 region (Fig. 3, E and F), and at high magnification was detected as a punctate pattern in the neuropil (inset in Fig. 3F). In these regions, the mean fluorescence intensity was significantly higher with GAA fixation than with PFA fixation (Fig. 3G). These labeling patterns are consistent with those obtained by in situ hybridization for GluN1 mRNA (*17*, *18*) and similar to those obtained after pepsin digestion of PFA-fixed sections (*5*, *19*–*21*), though at the much lower signal intensity in the latter. Improvement by GAA fixation was also observed in paraffin-embedded sections. Immunofluorescence signals for GluD2, an iGluR that is enriched at parallel fiber–Purkinje cell synapses, were greatly intensified in the cerebellar molecular layer of GAA-fixed paraffin sections, compared with PFA-fixed paraffin sections (fig. S5).

In electron microscopy, postembedding immunogold labeling is essential to visualize the postsynaptic localization of various iGluR members in PFA-fixed tissues (*4*, *14*, *19*, *22*, *23*), whereas pre-embedding immunogold labeling fails to detect AMPARs or NMDARs at synapses (Fig. 3H) (*4*). In GAA-fixed hippocampus, pre-embedding silver-enhanced immunogold clearly labeled postsynaptic sites at asymmetrical axo-spinous synapses in the hippocampus (Fig. 3, I to K). These results indicate that, in GAA-fixed tissue specimens, synaptic molecules become detectable by conventional protocols of pre-embedding immunohistochemistry at both the light and electron microscopic levels and that antigen-exposing techniques are no longer necessary. It should be noted that ultrastructural images were different in some respects between PFA- and GAA-fixed specimens; GAA fixation increased electron density and contrast at the cell membrane and organelles, while it decreased electron density and produced electron-lucent space in the cytoplasm (Fig. 3I).

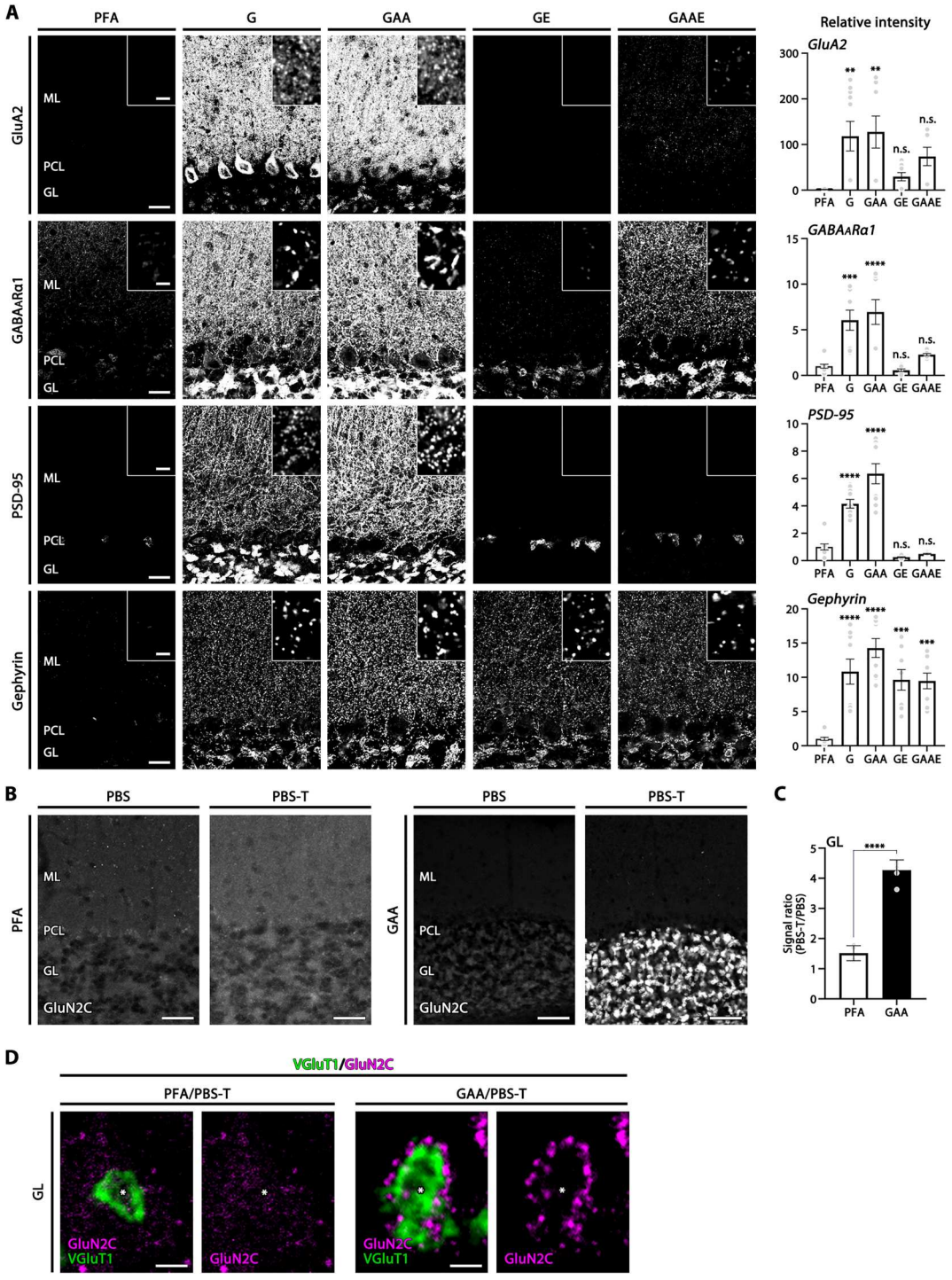

Fig. 1. Intensified immunofluorescence signals for postsynaptic molecules in glyoxal-fixed cerebellar cortex. (**A**) Immunofluorescence for AMPA receptor GluA2, $GABA_AR\alpha1$, excitatory postsynaptic scaffold protein PSD-95, and inhibitory postsynaptic scaffold protein gephyrin in tissues fixed by 4% PFA or glyoxal with different composition (see text). Insets indicate high-magnification images in the molecular layer. Histograms showing the mean relative fluorescent intensity in each glyoxal fixative normalized to that in 4% PFA. Each data point was calculated from 10 images per mouse ($n = 2$ mice). (**B**) Marked improvement of NMDAR GluN2C immunofluorescence detection in cerebellar glomeruli of glyoxal-fixed mouse sections by adding 0.1% Triton X-100 to PBS (PBS-T). In 4% PFA (PFA)–fixed sections, no specific signals are observed in the granular layer with the use of PBS or PBS-T. In 9% glyoxal/8% acetic acid (GAA)–fixed sections, use of PBS-T markedly intensifies GluN2C signals in the granular layer. (**C**) Histogram showing the mean signal ratio (PBS-T/PBS) in the granular layer with PFA fixation (six images from two mice) or GAA fixation (six images from two mice). (**D**) Double immunofluorescence for GluN2C (magenta) and VGluT1 (green) in cerebellar synaptic glomeruli. Use of PBS-T selectively intensifies GluN2C clusters that surround VGluT1(+) huge mossy fiber terminals (*) in GAA-fixed (right) but not PFA-fixed (left) sections. GL, granular layer; ML, molecular layer; PCL, Purkinje cell layer. Scale bars, 100 μm (B); 20 μm (A); 2 μm [A (inset) and D]. The data are shown as the means ± SEM. For detailed statistics see, Table S2 and S3.

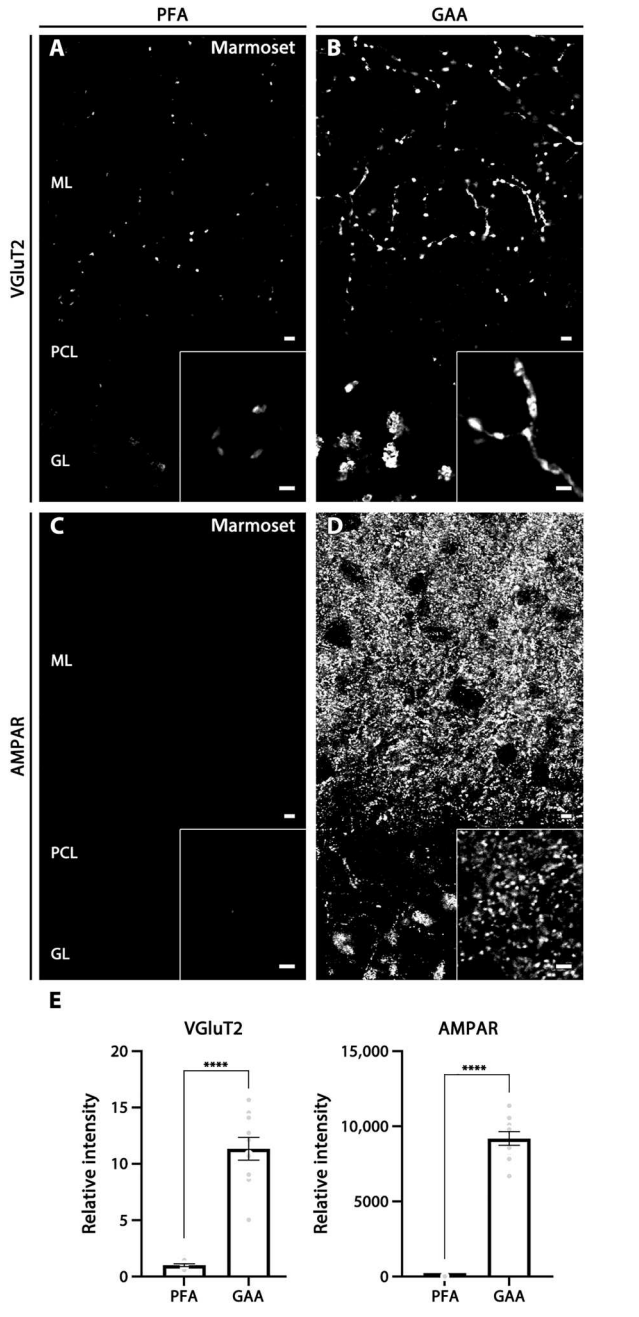

Fig. 2. Improved immunostaining by GAA fixation in the cerebellar cortex of marmoset brains. (**A** and **B**) VGluT2 labeling in PFA- (A) or GAA-fixed (B) cerebellum. (**C** and **D**) AMPAR labeling in PFA- (C) or GAA-fixed (D) cerebellum. Insets show enlarged images of the cerebellar molecular layer. (**E**) Histogram showing the mean relative ratio in GAA-fixed sections normalized to PFA-fixed sections in the cerebellar molecular layer (10 images from two marmosets). For detailed statistics, see Table S2 and S3. For abbreviations, see Fig. 1. Scale bars, 5 μm (A to D) (inset, 2 μm).

Deepening of molecular imaging

Even after antigen exposure, postsynaptic molecules deep in the section are still inaccessible in PFA-fixed tissues. For this reason, it is often difficult to simultaneously visualize apposing molecules in the same or adjacent compartments, for example, presynaptic transporters and postsynaptic receptors at single synapses. Improvement by GAA fixation was evaluated by stepwise *z*-axis acquisition of optical cerebellar sections immunostained for VGluT2 (a climbing fiber terminal marker), AMPAR (detected using a pan-AMPAR antibody), and calbindin (a Purkinje cell marker). In pepsin-undigested PFA-fixed sections, AMPAR signals were very faint in the molecular layer and were not associated with calbindin-labeled dendritic spines of Purkinje cells nor VGluT2-labeled climbing fiber terminals, suggesting that these signals were AMPARs on Bergmann glia (fig. S6). In pepsin-digested PFA-fixed sections, synaptic AMPARs on dendritic spines appeared on the surface of sections, but signal intensity dropped to the background level at 1-μm depth (Fig. 4, A to D and I). In GAA-fixed sections, the intensity for AMPARs as well as VGluT2 and calbindin signals was maintained at consistent levels to a much deeper region (1.8 μm from the section surface) (Fig. 4, E to H and J). As a result, high apposition rates between presynaptic VGluT2 and postsynaptic AMPAR were maintained at various depths of GAA-fixed sections (Fig. 4K).

We then used 100-μm-thick sections to test how deep immunosignals could be detected in GAA-fixed tissues. Signals for VGluT2, AMPARs, and calbindin were visible until 10 μm from the section surface but then dropped substantially (fig. S7, A, B, and D). To facilitate laser beam penetration into deep tissues, the tissue clearing method of Sca*l*eS was used after immunoreaction, by which immunosignals became detectable from deeper regions, such as at −30 μm deep from the section surface (Fig. 4, L and M, and fig. S7, C and E). Further deepening of immunofluorescence detection was achieved by using the tissue clearing method of AbSca*l*e during incubation of immunoreaction, by which intense immunosignals were evenly detected throughout the *xz* and *yz* axes of 100-μm-thick sections (Fig. 4, N and O, and fig. S7, C and F).

Increased signal intensity

In postembedding immunohistochemistry, antibodies can only access and bind epitopes exposed on the surface of ultrathin resin sections (~90 nm in thickness). By taking advantage of the limited antibody penetration, we directly tested effects of signal intensification by GAA fixation using postembedding methods. By immunofluorescence, signals for GluD2 were significantly intensified in the cerebellar molecular layer of GAA-fixed, Lowicryl-embedded ultrathin sections compared with PFA-fixed sections (fig. S8, A to E). This intensification was mainly caused by the increased size of individual fluorescent puncta but not by increased number or density of fluorescent puncta (fig. S8F). This signal intensification clearly visualized that GluD2 puncta faced to VGluT1-positive parallel fiber terminals (white arrowheads) but not to VGluT2-positive climbing fiber terminals (yellow arrows; Fig. 5, A and B). This input-selective allocation of GluD2 is consistent with conclusions from previous electron microscopic studies using postembedding immunogold labeling (*14*, *24*). When applied to postembedding immunogold electron microscopy, a significant increase in the labeling density of immunogold particles for GluD2 per unit length of the postsynaptic membrane was shown in GAA-fixed, Lowicryl-

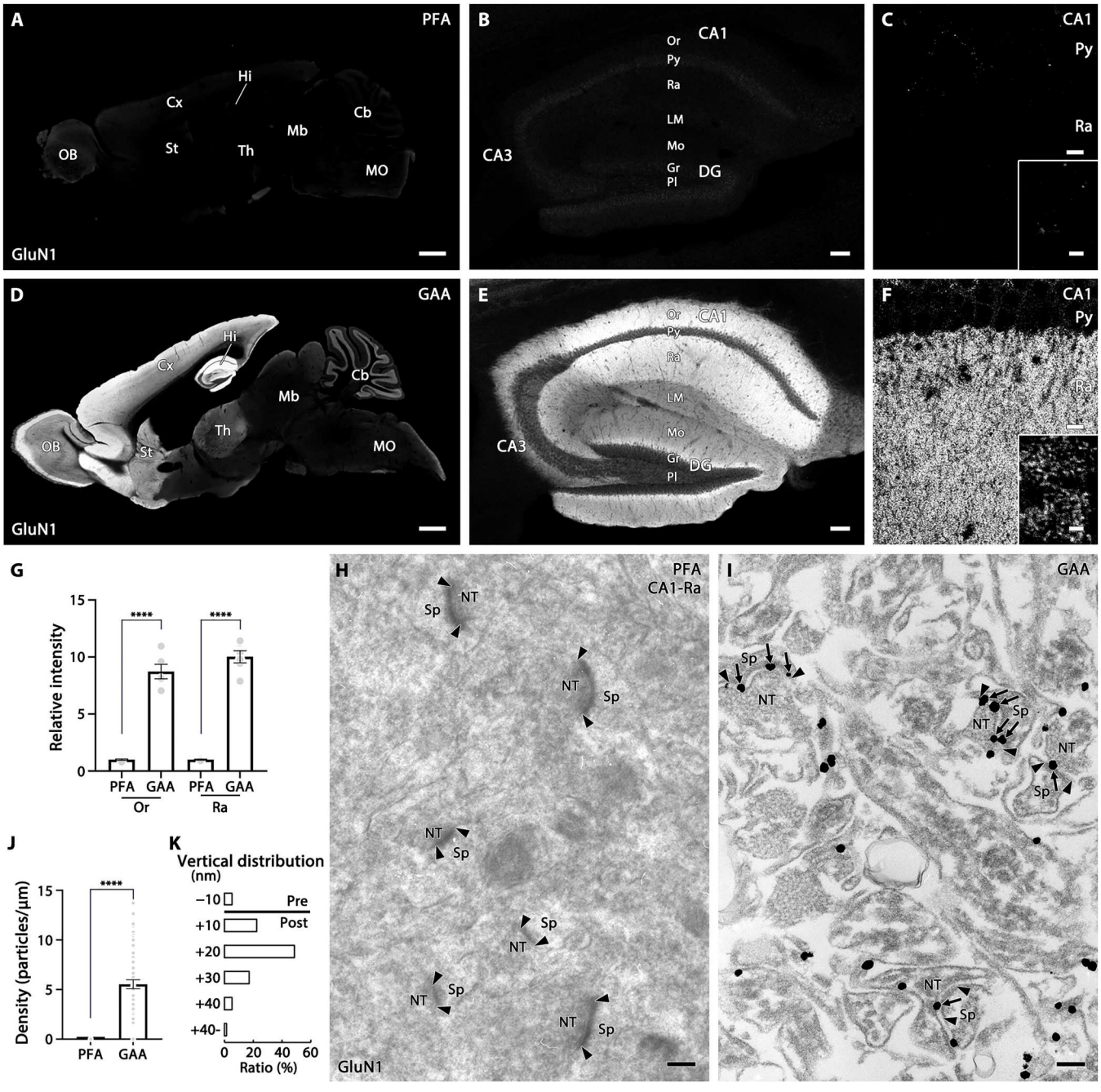

Fig. 3. Improved immunostaining for NMDAR GluN1 by GAA fixation of mouse brains. (**A** to **F**) Immunofluorescence in PFA- (A to C) or GAA-fixed (D to F) brain (A and D), hippocampus (B and E), and CA1 region (C and F). (**G**) Histogram showing the mean relative intensity in GAA-fixed sections normalized to PFA-fixed sections in the CA1 stratum oriens (Or) and radiatum (Ra). Data were calculated from three images per mouse ($n = 2$ mice). (**H** and **I**) Pre-embedding silver-enhanced immunogold labeling in the CA1 stratum radiatum in PFA- (H) or GAA-fixed (I) hippocampus. Arrows and arrowheads indicate immunogold labeling and the edge of the postsynaptic density, respectively. (**J**) Histogram showing the mean labeling density of immunogold particles for GluN1 per 1 μm of the postsynaptic membrane at axo-spinous synapses in PFA- ($n = 66$ synapses from two mice) or GAA-fixed ($n = 62$ synapses from two mice) CA1 stratum radiatum. (**K**) The vertical distribution of the center of immunoparticles ($n = 58$ particles from two mice) at axo-spinous synapses of GAA-fixed CA1 stratum radiatum. In the ordinate, − and + represent the presynaptic and postsynaptic side, respectively, from the midline of the synaptic cleft. The distribution of immunogold particles for GluN1 peaks in a +10- to +20-nm postsynaptic bin, with a mean distance of +14.7 ± 1.2 nm. For detailed statistics, see Table S2 and S3. CA1–3, CA1–3 regions of Ammon's horn; Cb, cerebellum; Cx, cortex; DG, dentate gyrus; Gr, granule cell layer; Hi, hippocampus; LM, stratum lacunosum-moleculare; Mb, midbrain; MO, medulla oblongata; Mo, molecular layer; NT, nerve terminal; OB, olfactory bulb; Or, stratum oriens; Pl, polymorphic cell layer; Py, pyramidal cell layer; Ra, stratum radiatum; Sp, spine; St, striatum; Th, thalamus. Scale bars, 1 mm (A and D); 100 μm (B and E); 10 μm (C and F) (inset, 2 μm); 200 nm (H and I).

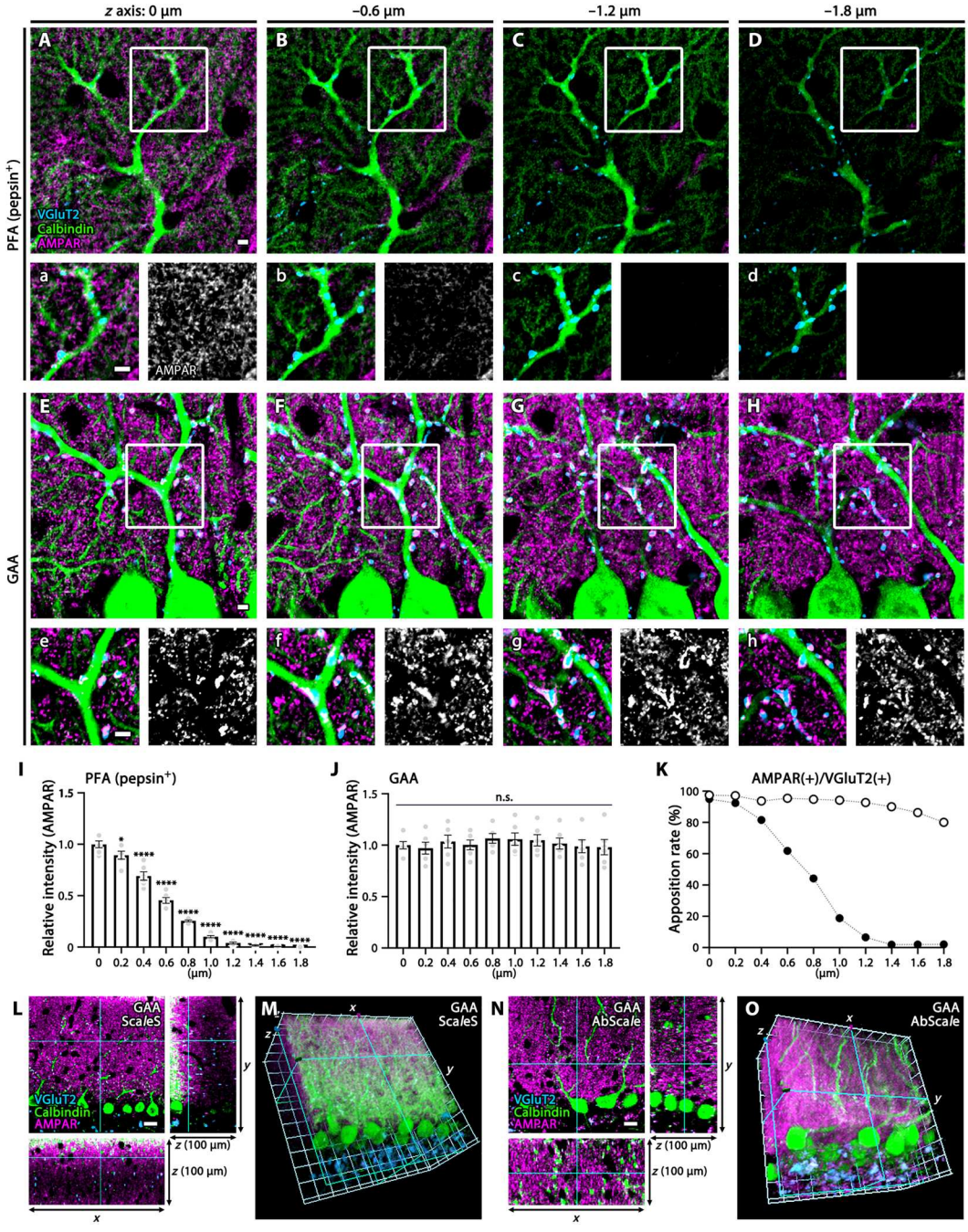

Fig. 4. Deep *z*-axis imaging of AMPAR by GAA fixation in the mouse cerebellar cortex. (**A** to **H** and **L** to **O**) Immunofluorescence for AMPAR (magenta), VGluT2 (blue), and calbindin (green) in PFA- (A to D) or GAA-fixed (E to H and L to O) cerebellar sections. PFA-fixed sections were subjected to pepsin digestion before immunostaining (A to D). Consecutive images along the *z* axis [0.2-μm steps, (A) to (H); 1-μm steps, (L) to (O)] were captured. Boxed regions in (A) to (H) are enlarged in (a) to (h), and AMPAR signals are separately shown in white. See also fig. S6 for faint surface signals of glial AMPAR in pepsin-undigested PFA-fixed sections and fig. S7 (D to F) for deeper imaging of synaptic AMPAR from the surface (0 μm) to −50 μm deep in GAA-fixed 100-μm-thick sections. (**I** and **J**) Histograms showing the mean relative intensity of AMPAR along the *z* axis (0 to −1.8-μm depth) in PFA- (I) or GAA-fixed (J) sections. The mean relative intensity at the surface is defined as 1.0, and statistically significant decreases at deeper regions are shown by $*P < 0.05$ and $****P < 0.0001$. Data were calculated from three images per mouse ($n = 2$ mice). (**K**) Histogram showing the apposition rate of VGluT2(+) presynaptic and AMPAR(+) postsynaptic puncta at 0 to −1.8 μm deep. The *xy*, *xz*, and *yz* planes of images (L and N) and 3D-recontructed images (M and O) of GAA-fixed 100-μm-thick cerebellar sections, to which the tissue clearing method of Sca*l*eS was applied after immunoreaction (L and M) or the tissue clearing method of AbSca*l*e was applied during immunoreaction (N and O). For detailed statistics, see Table S2 and S3. Scale bars, 20 μm (L and N); 10 μm (A to H).

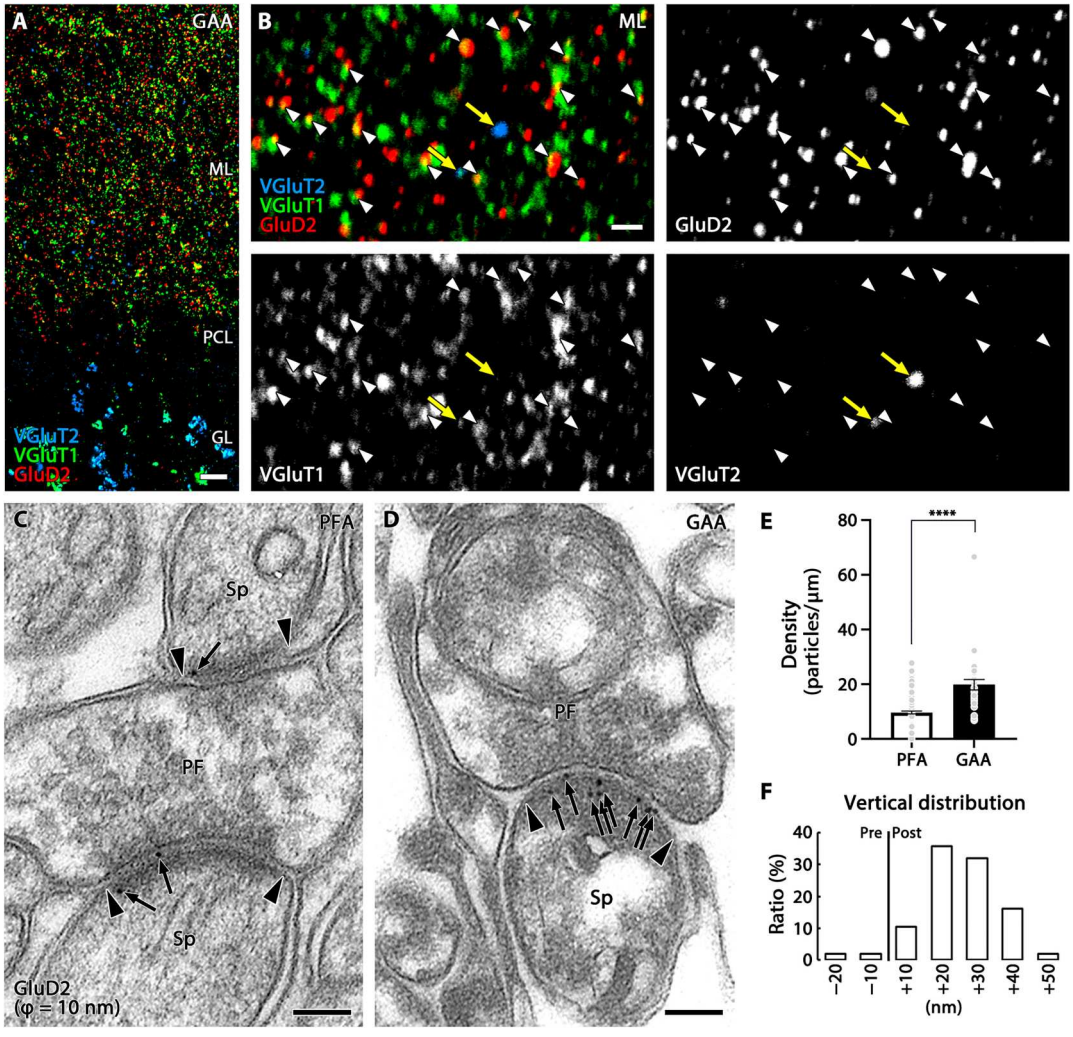

Fig. 5. Signal intensification in postembedding immunofluorescence and immunogold labeling of GluD2 in GAA-fixed mouse cerebellum. (**A** and **B**) Triple immunofluorescence for GluD2 (red), VGluT1 (green), and VGluT2 (blue) in ultrathin Lowicryl sections of GAA-fixed cerebellar cortex. Improved spatial resolution and signal intensity allow apposition of GluD2 clusters to VGluT1(+) parallel fiber terminals (white arrowheads), but not to VGluT2(+) climbing fiber terminals (yellow arrows), to be clearly demonstrated. (**C** and **D**) Post-embedding immunogold electron microscopy for GluD2 (ϕ = 10 nm) in PFA- (C) or GAA-fixed (D) ultrathin Lowicryl sections. Arrows and arrowheads indicate immunogold labeling and the edge of the postsynaptic density, respectively. (**E**) Histogram showing the mean density of immunogold particles for GluD2 per 1 μm of the postsynaptic membrane obtained from *n* = 159 synapses from two mice (PFA) and 32 synapses from two mice (GAA). (**F**) Histogram showing the vertical distribution of GluD2 immunogold at parallel fiber-Purkinje cell synapses in GAA-fixed ultrathin Lowicryl sections. See legend for Fig. 3K for measurement method. The distribution of immunogold particles (*n* = 106 particles from two mice) peaked in a +10- to +20-nm postsynaptic bin, with a mean distance of +19.54 ± 1.09 nm from the midline of the synaptic cleft. For detailed statistics, see Table S2 and S3. PF, parallel fiber terminal; Sp, dendritic spine. For other abbreviations, see Fig. 1. Scale bars, 10 μm (A); 2 μm (B); 100 nm (C and D).

embedded ultrathin sections (Fig. 5, C to F). Although the contrast of electron microscopic images was slightly different between PFA- and GAA-fixed specimens, the cell membrane, organelles, and synaptic junctions were identifiable in both specimens.

Reassessment of specific primary antibodies

The above notable results using GAA fixation prompted us to re-evaluate primary antibodies that had been judged to be useless because of poor signal yield in specificity tests using PFA-fixed brain sections. An antibody to the synaptic adhesion molecule, Neuroligin 1 (NL1), is one such antibody that was ineffective with PFA-fixed tissue but specific when used with GAA fixation (Fig. 6, A to G). The absence of immunostaining in NL1-knockout mouse brains (Fig. 6D, inset) verified the specificity of NL1 immunohistochemistry. The intensity of fluorescent signals for NL1 was comparable at PSD-95(+) excitatory and $GABA_AR\gamma2$(+) inhibitory synapses in the stratum radiatum of the hippocampal CA1, while it was higher at excitatory synapses than inhibitory synapses in the stratum lacunosum-moleculare of the hippocampal CA1 and in layers I and V of the cortex (Fig. 6, H to O). Pre-embedding silver-enhanced immunoelectron microscopy yielded specific NL1 labeling at postsynaptic sites of asymmetrical axo-spinous synapses in the CA1 stratum lacunosum-moleculare (Fig. 6, P to T).

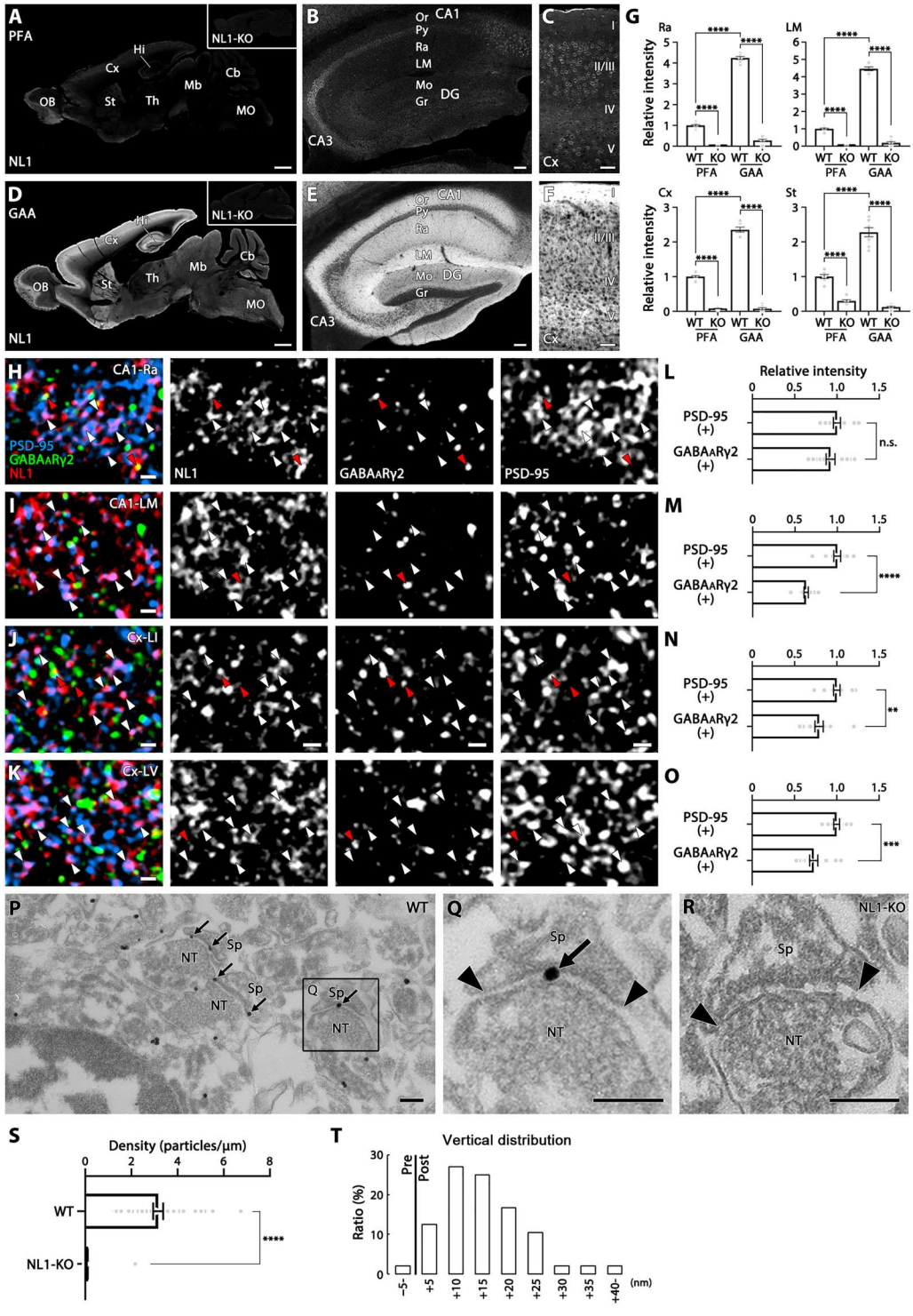

Fig. 6. Visualization of specific immunosignals for synaptic adhesion molecule NL1 in GAA-fixed mouse brains. (**A** to **F**) Immunofluorescence for NL1 in PFA- (A to C) or GAA-fixed (D to F) brain (A and D), hippocampus (B and E), and cortex (C and F). (**G**) Histograms showing that the mean relative intensity is significantly increased in GAA-fixed CA1 stratum radiatum, CA1 stratum lacunosum-moleculare, cortex, and striatum than in PFA-fixed ones. The intensity of PFA-fixed wild-type mice is defined as 1.0. Data were measured from five images per mouse (n = 2 mice). (**H** to **K**) Triple immunofluorescence for NL1 (red), PSD-95 (blue), and $GABA_AR\gamma2$ (green) in the stratum radiatum (H) and stratum lacunosum-moleculare (I) of the hippocampal CA1, and in layers 1 (J) and 5 (K) of the somatosensory cortex. White and red arrowheads indicate NL1 clusters that are apposed to PSD-95- or $GABA_AR\gamma2$-positive clusters, respectively. (**L** to **O**) Histograms showing that the mean relative intensity of NL1 clusters apposing to PSD-95(+) clusters or $GABA_AR\gamma2$(+) clusters in the CA1 stratum radiatum (L, PSD-95 clusters, n = 1567; $GABA_AR\gamma2$ clusters, n = 1049, from two mice), CA1 lacunosum-moleculare (M, 1801, 1436, from two mice), and in layer 1 (N, 1346, 1186 from, two mice) and layer 5 (O, 1393, 741, from two mice) of the somatosensory cortex. The intensity of NL1 clusters apposing to PSD-95 clusters is defined as 1.0. n.s., not significant. (**P** to **R**) Pre-embedding silver-enhanced immunogold labeling in the CA1 stratum radiatum in GAA-fixed wild-type (P and Q) or NL1-knockout (R) mice. Arrows and arrowheads indicate immunogold labeling and the edge of the postsynaptic density, respectively. (**S**) Histogram showing the mean labeling density of immunogold particles for NL1 per 1 μm of the postsynaptic membrane at axo-spinous synapses of GAA-fixed CA1 stratum radiatum in wild-type (n = 37 synapses from two mice) or NL1-knockout (n = 69 synapses from two mice) mice. (**T**) The vertical distribution of the center of immunoparticles (n = 48 particles from two mice) at axo-spinous synapses of GAA-fixed CA1 stratum radiatum. See legend for Fig. 3K for measurement method. For detailed statistics, see Table S2 and S3. For abbreviations, see Fig. 3. Scale bars, 1 mm (A and D); 100 μm (B and E); 50 μm (C and F); 1 μm (H to K); 200 nm (P to R).

Signal enhancement for various molecular categories

Last, we extended our tests to various molecular categories functioning in the brain. To this end, we tested commercial and in-house antibodies against 53 molecules, comprising 9 ionotropic receptors (GluA2, GluA3, GluK2, GluN2B, GluN2C, GluD1, GluD2, $GABA_AR\alpha1$, and $GABA_AR\gamma2$; Fig. 7), 3 voltage-gated ion channels (Nav1.x as detected using pan-$Na_V1.1$–1.9 antibody, Kv1.1, and Cav2.1; fig. S9), 2 auxiliary subunits of AMPARs (TARP-γ2 and TARP-γ8; fig. S10), 4 scaffold proteins of receptors and ion channels (Shank2, Homer-1, gephyrin, and ankyrin-G; fig. S10), 6 metabotropic receptors and related signaling molecules (mGluR1, $GABA_BR2$, mAChR1, D1R, IP_3R1, and PLCβ1; fig. S11), 6 vesicular transporters (VGluT1, VGluT2, VGluT3, VIAAT, VAChT, and VMAT2; fig. S12), 7 plasmalemmal transporters (GLAST, GAT1, GlyT2, CHT, DAT, NET, and HTT; fig. S13), 3 synaptic vesicle-associated and active zone proteins (Bassoon, CAST, and synapsin-1; fig. S14), 5 synaptic adhesion molecules (Cbln1, Cbln3, Nrxn1α, NL2, and NL3; fig. S15), 2 neuropeptides [somatostatin and vasoactive intestinal polypeptide (VIP); fig. S16], 3 cytosolic Ca^{2+}-binding proteins (calbindin, calretinin, and parvalbumin; fig. S17), and 3 glial marker proteins (Iba1, GFAP, and CNPase; fig. S18).

The mean fluorescence intensity, which was measured from appropriate neural regions, was significantly higher for 47 of these 53 molecules in GAA-fixed tissues than in PFA-fixed tissues (table S3). Iba1, however, was accompanied by increased background labeling in the neuropil (fig. S18) and was therefore omitted from significantly intensified cases. Signal levels in GAA-fixed tissues were judged to be comparable with those in PFA-fixed tissues for five molecules—mGluR1, mAChR1, synapsin-1, VIP, and parvalbumin—and to be significantly lower for somatostatin. In addition, significant augmentation by GAA fixation was already shown for four more molecules: PSD-95 (Fig. 1 and figs. S2 and S3), SAP-102 (fig. S3), GluN1 (Fig. 3), and NL1 (Fig. 6). Overall, significant signal intensification by GAA fixation was observed for 50 of 57 molecules (88%). In addition to GluN1 (fig. S4) and NL1 (Fig. 6, A and D, inset), the specificity of immunohistochemical signals was verified for GluD1, GluD2, PSD-95, NL2, and NL3 by negative labeling in knockout mouse brains (Fig. 8). These results indicate a broad usefulness of glyoxal fixation for neuroscience research targeting various categories of molecules.

DISCUSSION

To challenge the problem in the immunohistochemical detection of molecules that are buried in specialized neuronal compartments, we applied glyoxal fixation to adult mouse and marmoset brains, optimized the protocol for glyoxal-based immunohistochemistry, and compared the immunosignals produced with those produced using 4% PFA fixation. Here, we report substantial qualitative and quantitative improvements in the detection of various categories of molecules using glyoxal fixation.

Technical considerations

We confirmed the conclusion by Richter *et al.* (*11*) that immunohistochemical signals are intensified using glyoxal fixation and that adjustment of glyoxal fixative to pH 4 or 5 is essential to produce this effect. Our subsequent optimization trials highlighted several points. In the original glyoxal fixative, 20% ethanol was added because cell morphology is better preserved by speeding membrane penetration of fixative (*11*). We found, however, that glyoxal fixatives without ethanol yielded stronger intensification for many synaptic molecules compared with those containing 20% ethanol (Fig. 1 and fig. S1). Sections fixed by the original glyoxal fixative were soft and often broke or became deformed during free-floating incubation. This defect was worsened by the omission of acetic acid. We solved this fragility problem by increasing the concentration of glyoxal and acetic acid up to 9 and 8%, respectively. This achieved tissue hardening without loss of signal intensity (fig. S2). Differences in optimal conditions between the present study and that of Richter *et al.* (*11*) may, at least partly, be because Richter *et al.* (*11*) used cultured cells while we used tissue sections.

In conventional immunohistochemistry using formaldehyde-fixed sections, Triton X-100 is often added to the incubation buffer to facilitate antibody penetration into tissues, but its use is optional. In contrast, Triton X-100 was essential for glyoxal-based immunohistochemistry. We adopted the concentration of 0.1% Triton X-100, based on the finding that GluN2C labeling in cerebellar synaptic glomeruli was intense at this concentration, obscure without Triton X-100 (Fig. 1B), and in between at 0.01%. We also noted, however, that use of 0.1% Triton X-100 caused poor preservation of cell and organelle membranes when observed by pre-embedding immunoelectron microscopy in both glyoxal-fixed and 4% PFA–fixed brain tissues (Fig. 3, H and I).

Increased accessibility of antibody to antigen

Qualitative improvement of immunohistochemistry by glyoxal fixation was particularly remarkable for ionotropic receptors and their auxiliary subunit (iGluR, TARP, and $GABA_AR$), ion channels ($Na_V1.x$, $K_V1.1$, and $Ca_V2.1$), their scaffold proteins (PSD-95 protein family, gephyrin, and ankyrin-G), and synaptic adhesion molecules (Cbln, NL, and Nrxn). All these molecules are condensed and buried in specialized neuronal compartments (i.e., postsynapse, synaptic cleft, axon initial segment, and Ranvier's node), hardly detected in formaldehyde-fixed brain tissues by conventional immunohistochemistry, and require certain antigen-exposing techniques (*2*–*6*, *8*, *13*, *14*, *23*, *25*, *26*). The antigen-exposing techniques, such as pepsin pretreatment for light microscopy and postembedding immunogold labeling for electron microscopy, have contributed to uncovering the molecular localization at such specialized compartments. However, pepsin pretreatment was ineffective for GluD1 and $Ca_V2.1$. Instead, fresh frozen sections, which are prepared from unfixed tissues and fixed briefly with 4% PFA before immunohistochemical incubation, effectively showed specific GluD1 and $Ca_V2.1$ signals (*15*, *27*). Fritschy *et al.* (*6*) used microwave irradiation with formaldehyde fixation to detect iGluR and $GABA_AR$. Lorincz and Nusser (*7*) successfully demonstrated dendritic Na_V by formaldehyde fixation using a low concentration/low pH protocol. Thus, all these antigen-exposing techniques have been developed to overcome this problem. Unexpectedly, all these buried molecules in formaldehyde-fixed brain tissues were detectable in glyoxal-fixed tissues using conventional immunohistochemistry protocols.

This qualitative improvement suggests that the accessibility of antibodies to target molecules is greatly facilitated in glyoxal-fixed tissues. This assumption is substantiated by the finding that intense AMPARs signals were detected at much deeper levels in glyoxal-fixed compared with PFA-fixed sections (Fig. 4 and fig. S7). By combining glyoxal fixation with the tissue clearing method,

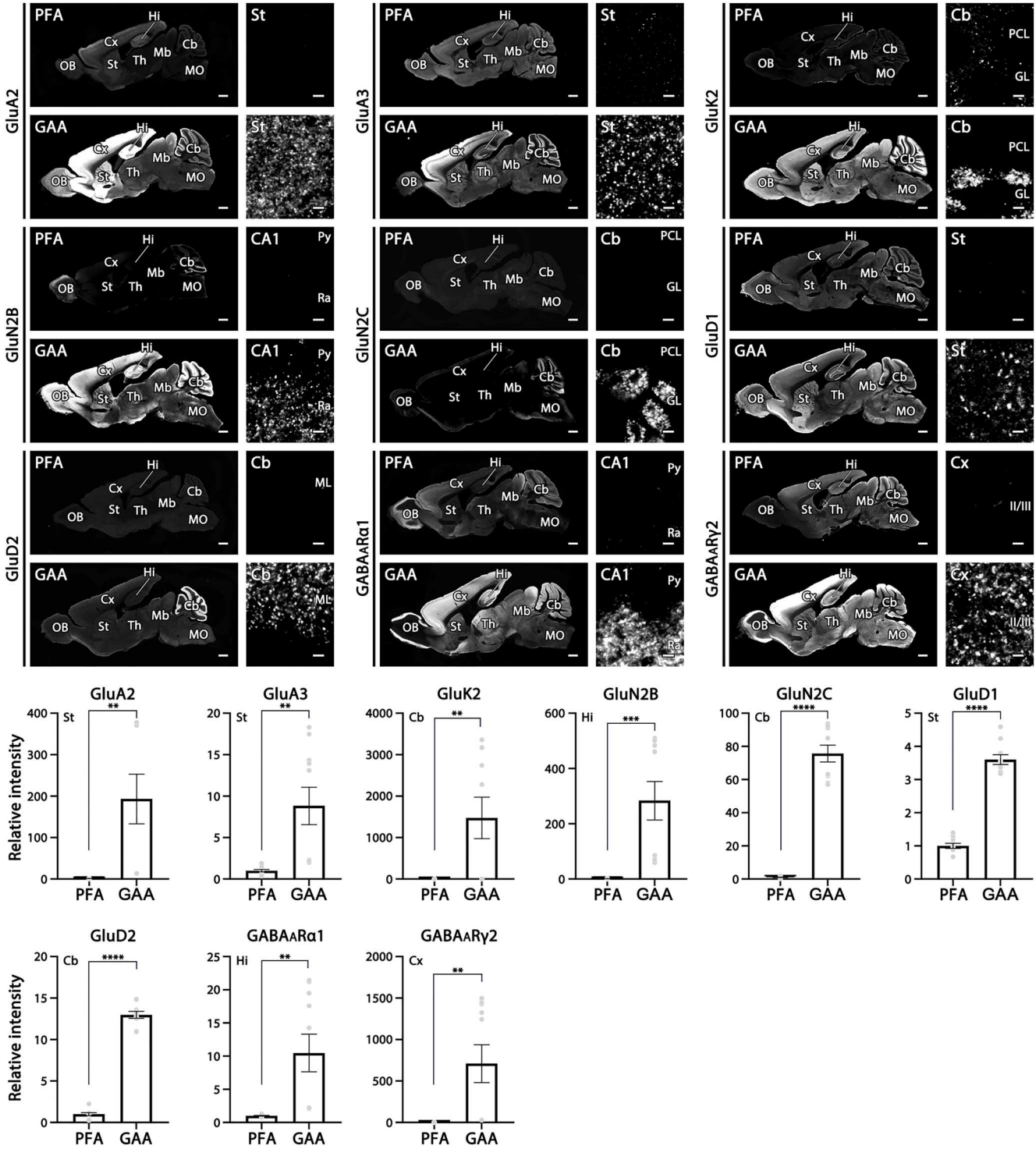

Fig. 7. Significant intensification of immunofluorescence signals for nine ionotropic receptors in the mouse brain. For each molecule, left panels show overall staining patterns in parasagittal brain sections and right panels show magnified images from representative regions of the brain. Compared with PFA fixation, the mean relative intensity is significantly increased by GAA fixation for AMPAR GluA2 in the striatum, AMPAR GluA3 in the striatum, kainate-type glutamate receptor GluK2 in the cerebellum, NMDAR GluN2B in hippocampal CA1, NMDAR GluN2C in the cerebellum, delta family GluD1 in the striatum, delta family GluD2 in the cerebellum, $GABA_AR\alpha1$ in hippocampal CA1, and $GABA_AR\gamma2$ in the somatosensory cortex. Data are the average of five images per mouse ($n = 2$ mice) and the total measured area was 0.14 mm^2. For detailed statistics, see Table S2 and S3. See Figs. 1 and Fig. 3 for abbreviations. Scale bars, 1 mm (low-magnification left panels) and 2 μm (high-magnification right panels).

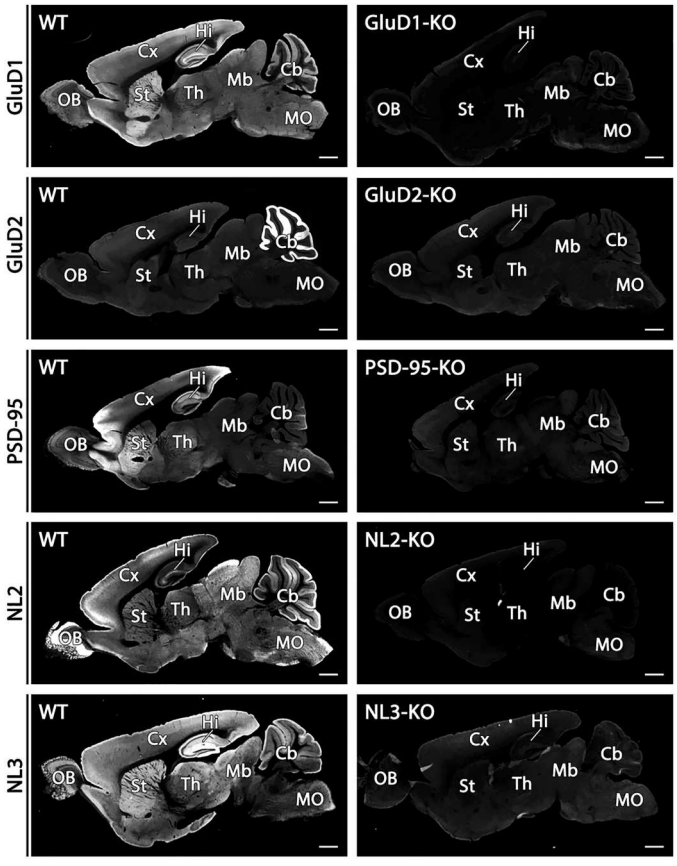

Fig. 8. Specificity for immunofluorescent signals for GluD1, GluD2, PSD-95, NL2, and NL3. The specificity of immunosignals in wild-type mouse brains is verified by the absence in respective knockout mouse brains. Scale bars, 1 mm.

punctate AMPAR labeling, together with VGluT2 and calbindin signals, was detectable at any depths of 100-μm-thick sections, indicating that the accessibility of antibodies is facilitated by fixation with glyoxal and further improved by combination with tissue clearing methods. This effect should increase the repertoire of detectable molecules by routine immunohistochemistry, enable more precise and efficient analysis of the spatial relationship of multiple molecules localized in the same or neighboring compartments, and facilitate the tracing of axons that wander, branch, and terminate in deep neural tissues.

Increase of antigenicity

Quantitative improvement by glyoxal fixation was also demonstrated for many other molecules that are detectable in formaldehyde-fixed tissues by conventional immunohistochemistry. These molecules include transmitter transporters on synaptic vesicles and cell membranes, metabotropic receptors and their downstream signaling molecules, active zone proteins, and glial marker proteins. The signal intensity of these molecules was enhanced to various degrees in glyoxal-fixed tissues. This quantitative improvement suggests that the antigenicity of molecules per se is enhanced by glyoxal fixation compared with formaldehyde fixation. Supporting this, post-embedding detection of GluD2 was improved, increasing the size of individual fluorescent puncta by immunofluorescence (fig. S8) and the labeling density of immunogold particles by postembedding electron microscopy (Fig. 5, C to E). These qualitative and quantitative improvements by glyoxal fixation were also observed in the marmoset brain (Fig. 2), expanding the utility of glyoxal fixation to various species of experimental animals.

Improvement of specificity

We tested glyoxal fixation for an NL1 antibody that showed no specific staining in PFA-fixed tissues. NL1 is a member of a major postsynaptic family of synaptic cell adhesion proteins that interact with presynaptic neurexins (*28*). All our eight in-house NL1 antibodies raised against different regions of the protein were judged to be useless, because no difference was found in immunohistochemical staining between formaldehyde-fixed wild-type and NL1-knockout brains, even using antigen-exposing techniques. Using glyoxal fixation, one antibody raised against the intracellular C-terminal region of NL1 yielded punctate labeling in wild-type but not in NL1-knockout brains (Fig. 6A to F). Similar cases were found for a commercial $GABA_AR\gamma2$ antibody (Fig. 7) and an in-house $GABA_BR2$ antibody (fig. S11), whose specificity was supported by reduced or blank labeling in neurons from small interfering RNA–mediated knockdown cerebella.

Chemical consideration

These substantial effects of glyoxal fixation prompt us to be aware of the potential loss of authentic or specific signals in formaldehyde-fixed tissues. What is the chemical basis for differences in antibody specificity and antigenicity of molecules caused by different aldehyde fixatives?

Glyoxal and glutaraldehyde are representative dialdehyde fixatives having two formyl (or aldehyde) groups, one at each end. Compared with formaldehyde, glyoxal fixation very often intensifies the immunosignal, whereas glutaraldehyde fixation diminishes it severely. Tissue hardness is also different among aldehyde fixatives; tissues fixed by glyoxal are soft, those fixed by glutaraldehyde are hard, and those fixed by formaldehyde are intermediate. In chemical structure, glyoxal differs from glutaraldehyde in the number of carbon atoms linking the two formyl groups (0 and 3, respectively). Likewise, glyoxal differs from formaldehyde in the number of formyl groups (2 and 1, respectively). It is speculated that the chemical structure of glyoxal endows it with exquisite cross-linking properties that preserve protein structure and antigenicity suitable for immunohistochemistry. Biophysical effects by aldehyde fixation upon protein conformation need to be comparatively investigated in the future.

Future directions

No significant signal intensification by glyoxal fixation was found for some molecules. Moreover, signal levels and noise were both increased in Iba1 labeling. It remains unknown whether and how differential signal intensification by glyoxal fixation depends on molecular species or whether it varies by epitope in the same molecule. Formaldehyde fixation is currently superior to glyoxal fixation with regard to ultrastructural images of neurons and synapses. Therefore, parallel use of formaldehyde and glyoxal is strongly recommended for immunohistochemistry, especially when testing primary antibodies for the first time.

Human tissue specimens are routinely fixed for pathological examination by immersion in 10% formalin and stored as paraffin

blocks and slides. We showed that intense signals for GluD2 could be obtained in glyoxal-fixed paraffin sections compared with signals from formaldehyde-fixed sections (fig. S5). Faster cell penetration and fixation properties of glyoxal (*11*) as well as similar improving effect upon marmoset brains (Fig. 2) suggest that the use of glyoxal fixation with autopsied human samples will facilitate pathological diagnosis and medical research by enhancing the sensitivity and specificity of immunostaining. Furthermore, if glyoxal fixation is also effective with non-neural tissues and organs, then it will contribute widely to life science research.

MATERIALS AND METHODS

Animals

We used adult C57BL/6, PV-Cre (Jackson Laboratory), GluN1-flox (Jackson Laboratory), and knockout mice for GluD1 (*16*), GluD2 (*29*), NL1, NL2, NL3, and PSD-95 (Jackson Laboratory), each mouse at 2 to 3 months of age. In each experiment, we used three male mice for qualitative and quantitative analyses. We also used adult common marmosets (*Callithrix jacchus*), which were purchased from CLEA Japan Inc. (Tokyo, Japan) and housed under 12-hour light/dark cycle (light on at 08:00, off at 20:00), with free access to food and water, at a temperature maintained at 28°C. All experiments were performed according to the guidelines laid down by the animal welfare committees of Hokkaido University, Niigata University, University of Massachusetts Medical School, Yale University, and the University of Tokyo.

Antibodies and reagents

In the present study, we produced affinity-purified antibodies against the following mouse molecules: $GABA_BR2$ (amino acid residues 858 to 890, GenBank NM_001081141.2), NL1 (805 to 826, NM_138666.3), somatostatin (35 to 88, BC010770.1), synapsin-1 (686 to 706, NM_013680.4), and VIP (52 to 78, XM_006512446.1) according to previous studies (*5*, *30*). The antigen sequences for somatostatin and VIP were selected from their proforms to label both perikarya and axon terminals of expressing neurons. The specificity of these antibodies was verified by complete overlap of cell bodies labeled by immunofluorescence and fluorescent in situ hybridization for these neuropeptides and their transcripts, respectively. Information on the primary antibodies used is summarized in table S1. These primary antibodies were used at 1 μg/ml for immunofluorescence and pre-embedding silver-enhanced immunogold electron microscopy and at 20 μg/ml for postembedding immunogold electron microscopy.

PFA (Merck, 104005), glyoxal (40% solution, Sigma-Aldrich, 128465), acetic acid (FUJIFILM Wako Pure Chemical, 017-00256), ethanol (99.5%, FUJIFILM Wako Pure Chemical, 057 to 00456), Tris-aminomethane 999 (FUJIFILM Wako Pure Chemical, 011-16381), dibasic sodium phosphate ($Na_2HPO_4/12H_2O$, FUJIFILM Wako Pure Chemical, 193-02845), and monobasic sodium phosphate ($NaH_2PO_4/2H_2O$, FUJIFILM Wako Pure Chemical, 192-02815) were used.

Fixatives

The original glyoxal fixative reported by Richter *et al.* (*11*) was 3% (v/v) glyoxal/0.8% (v/v) acetic acid/20% (v/v) ethanol (pH 4 or 5). In the present study, we tested five kinds of glyoxal fixative; 3% glyoxal, 3% glyoxal/0.8% acetic acid, 9% glyoxal/8% acetic acid, 3% glyoxal/20% ethanol, and 3% glyoxal/0.8% acetic acid/20% ethanol. pH of glyoxal fixatives was adjusted to 4.0 by adding drops of 5 N NaOH.

FA stock solution (8%, w/v) was prepared by dissolving 80 g of PFA powder in 1 liter of H_2O prewarmed to 80°C and containing 1 ml of 5 N NaOH, followed by filtration through a filter paper (Advantec). Phosphate buffer (PB; pH 7.2) (0.2 M) was prepared by dissolving 58 g of $Na_2HPO_4/12H_2O$ and 6 g of $NaH_2PO_4/2H_2O$ in 1 liter of H_2O. 4% or 1% PFA in 0.1 M PB was prepared by mixing 8% PFA stock solution and 0.2 M PB.

Fixation and section preparation

Under deep pentobarbital anesthesia (100 mg/kg body weight, intraperitoneally), experimental animals were perfused transcardially with saline, followed by two volumes of body weight (e.g., 60 ml for mice weighing 30 g) of PFA or glyoxal fixative. Brains excised from the skull were further postfixed overnight in the same fixatives at 4°C. After immersion in 30% sucrose in 0.1 M PB, cryosections (50 μm thick) were prepared on a cryostat (CM1900, Leica Microsystems) and used for pre-embedding immunofluorescence and immunoelectron microscopy. Cryostat sections were incubated in borosilicated test tubes in the free-floating state. For tissue clearing, microslicer sections (100 μm thick) were prepared on a vibrating blade microtome (VT1000S, Leica).

To prepare paraffin sections, 4% PFA– and glyoxal-fixed brains were dehydrated in a series of graded alcohols and xylene and embedded in the same paraffin blocks. Paraffin sections (5 μm) were prepared on a sliding microtome (SM2000R, Leica Microsystems), floated onto a water bath, mounted on silane-coated glass slides (New Silane II, Muto Pure Chemicals), and dried on a heating plate. Sections were dewaxed in xylene and rehydrated in graded alcohols. For routine antigen retrieval, paraffin sections on glass slides were heated to 95°C in 1:200-diluted Immunosaver (10% sodium citraconic acid solution, Nisshin EM) for 30 min.

For postembedding immunofluorescence and immunogold electron microscopy, microslicer sections (400 μm) were cryoprotected by immersion in 30% glycerol in PB for 30 min and then frozen rapidly in liquid propane in an EM CPC unit (Leica Microsystems). Frozen sections were immersed in 0.5% uranyl acetate in methanol at −90°C in an AFS freeze-substitution unit (Leica Microsystems), infiltrated at −45°C with Lowicryl HM-20 resin (Electron Microscopy Sciences), which was then polymerized with ultraviolet light. Ultrathin sections were cut using an Ultracut ultramicrotome (Leica Microsystems) and mounted on nickel grids for electron microscopy or on silane-coated glass slides (New Silane II) for immunofluorescence.

Tissue clearing

SCALEVIEW-S Trial Kit was purchased from FUJIFILM Wako Chemicals. Two different tissue-clearing methods were applied to GAA-fixed 100-μm-thick sections for different purposes. The Sca*l*eS method was used after immunoreaction, to facilitate laser beam penetration to deep tissues without affecting antibody penetration. The AbSca*l*e method was used during immunoreaction, to facilitate both laser beam penetration and antibody penetration into deep tissues. Both methods were performed according to manufacturer's protocols (FUJIFILM Wako Chemicals).

Immunofluorescence

All immunohistochemical incubations were performed at room temperature except for tissue-clearing method. Unless otherwise noted, phosphate-buffered saline (pH 7.4) containing 0.1% Triton X-100 (PBS-T) was used as incubation and washing buffers. Sections were incubated with 10% normal donkey serum for 20 min, with primary antibody overnight, and with Cy3-labeled species-specific secondary antibodies (Jackson ImmunoResearch) for 2 hours. For double or triple immunofluorescence, sections were incubated with a mixture of primary antibodies overnight, and a mixture of Alexa 488–, Cy3-, and Alexa 647-labeled species-specific secondary antibodies (1:200 dilution; Invitrogen; Jackson ImmunoResearch) for 2 hours. Images of given brain regions were taken with a confocal laser-scanning microscope equipped with 473, 559, and 647 diode laser lines, and UPlanSApo (10×/0.40), UPlanSApo (20×/0.75), and PlanApoN (60×/1.4, oil immersion) objective lenses (FV1200; Olympus). Whole-brain images were constructed by stitching individual images taken with a light microscope (BZ-X710; Keyence) with PlanApo (4×/0.20) objective lenses (Nikon). The intensity of immunofluorescence signals in given brain regions or whole brains was measured by setting microscopes at the same gain level for given molecules. The numbers of images and mice analyzed are indicated in the figure legends.

Immunoelectron microscopy

For pre-embedding immunoelectron microscopy, PBS-T was used as incubation and washing buffers. Cryosections were incubated in 10% normal goat serum (Nichirei) for 30 min and then with primary antibody overnight. Secondary antibodies linked to 1.4-nm gold particles (Nanogold; Nanoprobes) were incubated for 2 hours and immunogold particles were intensified with a silver enhancement kit (silver enhancement reagents, Aurion). Sections were further postfixed with 2% PFA and 2% glutaraldehyde in 0.1 M PB for 12 hours and treated with 1% osmium tetroxide for 15 min, stained with 2% uranyl acetate for 30 min, dehydrated, and embedded in Epon 812.

For postembedding immunoelectron microscopy, tris-buffered saline (pH 7.4) containing 0.1% Triton X-100 (TBS-T) was used as incubation and washing buffers. Ultrathin sections on nickel grids were successively treated with the following solutions: 50 mM glycine for 10 min, blocking solution [2% normal goat serum (Nichirei)] for 10 min, rabbit anti-GluD2 antibody (20 μg/ml) diluted in blocking solution overnight, and colloidal gold-conjugated (10 nm) anti-rabbit immunoglobulin G (1:100, British BioCell International) diluted in blocking solution for 2 hours. After extensive washing in distilled water, sections were fixed with 2% OsO_4 for 15 min and stained with 5% uranyl acetate/40% ethanol for 90 s and Reynold's lead citrate solution for 60 s. Photographs of parallel fiber–Purkinje cell synapses were taken from the molecular layer of the cerebellum with an H-7100 electron microscope (Hitachi).

For quantitative analysis, the density of postsynaptic membrane–associated immunogold particles, which were defined as those <20 nm from the cell membrane, was counted on electron micrographs and analyzed using MetaMorph software (Molecular Devices). The vertical distribution at synapses was examined by sampling synaptic profiles whose presynaptic and postsynaptic membranes were cut perpendicularly to the plane of the synaptic cleft, and by measuring the distance from the midline of the synaptic cleft to the center of an immunogold particle.

Supplementary Materials

This PDF file includes:

Supplementary Text
Figs. S1 to S18
Tables S1 to S3
References

REFERENCES AND NOTES

1. K. Konno, M. Watanabe, Immunohistochemistry for ion channels and their interacting molecules: Tips for improving antibody accessibility, in *Receptor and Ion Channel Detection in the Brain. Methods and Protocols* (Neuromethods, Springer, 2016), vol. 110, pp. 171–178.
2. A. Lorincz, Z. Nusser, Cell-type-dependent molecular composition of the axon initial segment. *J. Neurosci.* **28**, 14329–14340 (2008).
3. A. Baude, E. Molnár, D. Latawiec, R. A. McIlhinney, P. Somogyi, Synaptic and nonsynaptic localization of the GluR1 subunit of the AMPA-type excitatory amino acid receptor in the rat cerebellum. *J. Neurosci.* **14**, 2830–2843 (1994).
4. A. Baude, Z. Nusser, E. Molnár, R. A. McIlhinney, P. Somogyi, High-resolution immunogold localization of AMPA type glutamate receptor subunits at synaptic and non-synaptic sites in rat hippocampus. *Neuroscience* **69**, 1031–1055 (1995).
5. M. Watanabe, M. Fukaya, K. Sakimura, T. Manabe, M. Mishina, Y. Inoue, Selective scarcity of NMDA receptor channel subunits in the stratum lucidum (mossy fibre-recipient layer) of the mouse hippocampal CA3 subfield. *Eur. J. Neurosci.* **10**, 478–487 (1998).
6. J. M. Fritschy, O. Weinmann, A. Wenzel, D. Benke, Synapse-specific localization of NMDA and $GABA_A$ receptor subunits revealed by antigen-retrieval immunohistochemistry. *J. Comp. Neurol.* **390**, 194–210 (1998).
7. A. Lorincz, Z. Nusser, Molecular identity of dendritic voltage-gated sodium channels. *Science* **328**, 906–909 (2010).
8. M. Fukaya, M. Watanabe, Improved immunohistochemical detection of postsynaptically located PSD-95/SAP90 protein family by protease section pretreatment: A study in the adult mouse brain. *J. Comp. Neurol.* **426**, 572–586 (2000).
9. G. K. McMaster, G. G. Carmichael, Analysis of single- and double-stranded nucleic acids on polyacrylamide and agarose gels by using glyoxal and acridine orange. *Proc. Natl. Acad. Sci. U.S.A.* **74**, 4835–4838 (1977).
10. D. D. Sabatini, K. Bensch, R. J. Barrnett, Cytochemistry and electron microscopy. The preservation of cellular ultrastructure and enzymatic activity by aldehyde fixation. *J. Cell Biol.* **17**, 19–58 (1963).
11. K. N. Richter, N. H. Revelo, K. J. Seitz, M. S. Helm, D. Sarkar, R. S. Saleeb, E. D'Este, J. Eberle, E. Wagner, C. Vogl, D. F. Lazaro, F. Richter, J. Coy-Vergara, G. Coceano, E. S. Boyden, R. R. Duncan, S. W. Hell, M. A. Lauterbach, S. E. Lehnart, T. Moser, T. F. Outeiro, P. Rehling, B. Schwappach, I. Testa, B. Zapiec, S. O. Rizzoli, Glyoxal as an alternative fixative to formaldehyde in immunostaining and super-resolution microscopy. *EMBO J.* **37**, 139–159 (2018).
12. T. Miyazaki, M. Fukaya, H. Shimizu, M. Watanabe, Subtype switching of vesicular glutamate transporters at parallel fibre-Purkinje cell synapses in developing mouse cerebellum. *Eur. J. Neurosci.* **17**, 2563–2572 (2003).
13. M. Uchigashima, T. Ohtsuka, K. Kobayashi, M. Watanabe, Dopamine synapse is a neuroligin-2-mediated contact between dopaminergic presynaptic and GABAergic postsynaptic structures. *Proc. Natl. Acad. Sci. U.S.A.* **113**, 4206–4211 (2016).
14. A. S. Landsend, M. Amiry-Moghaddam, A. Matsubara, L. Bergersen, S. Usami, R. J. Wenthold, O. P. Ottersen, Differential localization of delta glutamate receptors in the rat cerebellum: Coexpression with AMPA receptors in parallel fiber-spine synapses and absence from climbing fiber-spine synapses. *J. Neurosci.* **17**, 834–842 (1997).
15. K. Konno, K. Matsuda, C. Nakamoto, M. Uchigashima, T. Miyazaki, M. Yamasaki, K. Sakimura, M. Yuzaki, M. Watanabe, Enriched expression of GluD1 in higher brain regions and its involvement in parallel fiber-interneuron synapse formation in the cerebellum. *J. Neurosci.* **34**, 7412–7424 (2014).
16. C. Nakamoto, K. Konno, T. Miyazaki, E. Nakatsukasa, R. Natsume, M. Abe, M. Kawamura, Y. Fukazawa, R. Shigemoto, M. Yamasaki, K. Sakimura, M. Watanabe, Expression mapping, quantification, and complex formation of GluD1 and GluD2 glutamate receptors in adult mouse brain. *J. Comp. Neurol.* **528**, 1003–1027 (2020).
17. M. Watanabe, Y. Inoue, K. Sakimura, M. Mishina, Developmental changes in distribution of NMDA receptor channel subunit mRNAs. *Neuroreport* **3**, 1138–1140 (1992).

18. M. Watanabe, Y. Inoue, K. Sakimura, M. Mishina, Distinct distributions of five N-methyl-D-aspartate receptor channel subunit mRNAs in the forebrain. *J. Comp. Neurol.* **338**, 377–390 (1993).
19. M. Abe, M. Fukaya, T. Yagi, M. Mishina, M. Watanabe, K. Sakimura, NMDA receptor GluR-epsilon/NR2 subunits are essential for postsynaptic localization and protein stability of GluRzeta1/NR1 subunit. *J. Neurosci.* **24**, 7292–7304 (2004).
20. K. Akashi, T. Kakizaki, H. Kamiya, M. Fukaya, M. Yamasaki, M. Abe, R. Natsume, M. Watanabe, K. Sakimura, NMDA receptor GluN2B (GluR epsilon 2/NR2B) subunit is crucial for channel function, postsynaptic macromolecular organization, and actin cytoskeleton at hippocampal CA3 synapses. *J. Neurosci.* **29**, 10869–10882 (2009).
21. K. Yamada, M. Fukaya, H. Shimizu, K. Sakimura, M. Watanabe, NMDA receptor subunits GluRepsilon1, GluRepsilon3 and GluRzeta1 are enriched at the mossy fibre-granule cell synapse in the adult mouse cerebellum. *Eur. J. Neurosci.* **13**, 2025–2036 (2001).
22. J. G. Valtschanoff, A. Burette, R. J. Wenthold, R. J. Weinberg, Expression of NR2 receptor subunit in rat somatic sensory cortex: Synaptic distribution and colocalization with NR1 and PSD-95. *J. Comp. Neurol.* **410**, 599–611 (1999).
23. M. Yamasaki, M. Fukaya, M. Yamazaki, H. Azechi, R. Natsume, M. Abe, K. Sakimura, M. Watanabe, TARP γ-2 and γ-8 differentially control AMPAR density across schaffer collateral/commissural synapses in the hippocampal CA1 area. *J. Neurosci.* **36**, 4296–4312 (2016).
24. T. Takeuchi, T. Miyazaki, M. Watanabe, H. Mori, K. Sakimura, M. Mishina, Control of synaptic connection by glutamate receptor delta2 in the adult cerebellum. *J. Neurosci.* **25**, 2146–2156 (2005).
25. A. Iwakura, M. Uchigashima, T. Miyazaki, M. Yamasaki, M. Watanabe, Lack of molecular-anatomical evidence for GABAergic influence on axon initial segment of cerebellar Purkinje cells by the pinceau formation. *J. Neurosci.* **32**, 9438–9448 (2012).
26. M. Yamazaki, M. Fukaya, K. Hashimoto, M. Yamasaki, M. Tsujita, M. Itakura, M. Abe, R. Natsume, M. Takahashi, M. Kano, K. Sakimura, M. Watanabe, TARPs gamma-2 and gamma-7 are essential for AMPA receptor expression in the cerebellum. *Eur. J. Neurosci.* **31**, 2204–2220 (2010).
27. T. Miyazaki, M. Yamasaki, K. Hashimoto, M. Yamazaki, M. Abe, H. Usui, M. Kano, K. Sakimura, M. Watanabe, $Ca_v2.1$ in cerebellar Purkinje cells regulates competitive excitatory synaptic wiring, cell survival, and cerebellar biochemical compartmentalization. *J. Neurosci.* **32**, 1311–1328 (2012).
28. K. Ichtchenko, Y. Hata, T. Nguyen, B. Ullrich, M. Missler, C. Moomaw, T. C. Südhof, Neuroligin 1: A splice site-specific ligand for beta-neurexins. *Cell* **81**, 435–443 (1995).
29. M. Yamasaki, T. Miyazaki, H. Azechi, M. Abe, R. Natsume, T. Hagiwara, A. Aiba, M. Mishina, K. Sakimura, M. Watanabe, Glutamate receptor δ2 is essential for input pathway-dependent regulation of synaptic AMPAR contents in cerebellar Purkinje cells. *J. Neurosci.* **31**, 3362–3374 (2011).
30. M. Watanabe, Production of high-quality antibodies for the study of receptors and ion channels, in *Receptor and Ion Channel Detection in the Brain. Methods and Protocols* (Neuromethods, Springer, 2016), vol. 110, pp. 3–18.
31. E. Miura, M. Fukaya, T. Sato, K. Sugihara, M. Asano, K. Yoshioka, M. Watanabe, Expression and distribution of JNK/SAPK-associated scaffold protein JSAP1 in developing and adult mouse brain. *J. Neurochem.* **97**, 1431–1446 (2006).
32. T. Miyazaki, M. Yamasaki, K. F. Tanaka, M. Watanabe, Compartmentalized input-output organization of lugaro cells in the cerebellar cortex. *Neuroscience* **462**, 89–105 (2021).
33. E. Miura, K. Matsuda, J. I. Morgan, M. Yuzaki, M. Watanabe, Cbln1 accumulates and co-localizes with Cbln3 and GluRdelta2 at parallel fiber-Purkinje cell synapses in the mouse cerebellum. *Eur. J. Neurosci.* **29**, 693–706 (2009).
34. T. Iijima, E. Miura, K. Matsuda, Y. Kamekawa, M. Watanabe, M. Yuzaki, Characterization of a transneuronal cytokine family Cbln - regulation of secretion by heteromeric assembly. *Eur. J. Neurosci.* **25**, 1049–1057 (2007).
35. M. Narushima, M. Uchigashima, K. Hashimoto, M. Watanabe, M. Kano, Depolarization-induced suppression of inhibition mediated by endocannabinoids at synapses from fast-spiking interneurons to medium spiny neurons in the striatum. *Eur. J. Neurosci.* **24**, 2246–2252 (2006).
36. M. Uchigashima, M. Narushima, M. Fukaya, I. Katona, M. Kano, M. Watanabe, Subcellular arrangement of molecules for 2-arachidonoyl-glycerol-mediated retrograde signaling and its physiological contribution to synaptic modulation in the striatum. *J. Neurosci.* **27**, 3663–3676 (2007).
37. R. Ichikawa, M. Yamasaki, T. Miyazaki, K. Konno, K. Hashimoto, H. Tatsumi, Y. Inoue, M. Kano, M. Watanabe, Developmental switching of perisomatic innervation from climbing fibers to basket cell fibers in cerebellar Purkinje cells. *J. Neurosci.* **31**, 16916–16927 (2011).
38. K. Hisano, M. Watanabe, Y. Morimoto, Protective effects of the free radical scavenger edaravone against glutamate neurotoxicity in nearly pure neuronal culture. *J. Anesth.* **23**, 363–369 (2009).
39. T. Shibata, K. Yamada, M. Watanabe, K. Ikenaka, K. Wada, K. Tanaka, Y. Inoue, Glutamate transporter GLAST is expressed in the radial glia-astrocyte lineage of developing mouse spinal cord. *J. Neurosci.* **17**, 9212–9219 (1997).
40. M. Fukaya, M. Tsujita, M. Yamazaki, E. Kushiya, M. Abe, K. Akashi, R. Natsume, M. Kano, H. Kamiya, M. Watanabe, K. Sakimura, Abundant distribution of TARP γ-8 in synaptic and extrasynaptic surface of hippocampal neurons and its major role in AMPA receptor expression on spines and dendrites. *Eur. J. Neurosci.* **24**, 2177–2190 (2006).
41. G. G. Nagy, M. Al-Ayyan, D. Andrew, M. Fukaya, M. Watanabe, A. J. Todd, Widespread expression of the AMPA receptor GluR2 subunit at glutamatergic synapses in the rat spinal cord and phosphorylation of GluR1 in response to noxious stimulation revealed with an antigen-unmasking method. *J. Neurosci.* **24**, 5766–5777 (2004).
42. D. Yan, M. Yamasaki, C. Straub, M. Watanabe, S. Tomita, Homeostatic control of synaptic transmission by distinct glutamate receptors. *Neuron* **78**, 687–699 (2013).
43. M. Hondo, N. Furutani, M. Yamasaki, M. Watanabe, T. Sakurai, Orexin neurons receive glycinergic innervations. *PLOS ONE* **6**, e25076 (2011).
44. M. Nakamura, K. Sato, M. Fukaya, K. Araishi, A. Aiba, M. Kano, M. Watanabe, Signaling complex formation of phospholipase Cbeta4 with metabotropic glutamate receptor type 1alpha and 1,4,5-trisphosphate receptor at the perisynapse and endoplasmic reticulum in the mouse brain. *Eur. J. Neurosci.* **20**, 2929–2944 (2004).
45. J. Somogyi, A. Baude, Y. Omori, H. Shimizu, S. El Mestikawy, M. Fukaya, R. Shigemoto, M. Watanabe, P. Somogyi, GABAergic basket cells expressing cholecystokinin contain vesicular glutamate transporter type 3 (VGLUT3) in their synaptic terminals in hippocampus and isocortex of the rat. *Eur. J. Neurosci.* **19**, 552–569 (2004).
46. M. Narushima, M. Uchigashima, M. Fukaya, M. Matsui, T. Manabe, K. Hashimoto, M. Watanabe, M. Kano, Tonic enhancement of endocannabinoid-mediated retrograde suppression of inhibition by cholinergic interneuron activity in the striatum. *J. Neurosci.* **27**, 496–506 (2007).
47. J. Tanaka, S. Nakagawa, E. Kushiya, M. Yamasaki, M. Fukaya, T. Iwanaga, M. I. Simon, K. Sakimura, M. Kano, M. Watanabe, Gq protein alpha subunits Galphaq and Galpha11 are localized at postsynaptic extra-junctional membrane of cerebellar Purkinje cells and hippocampal pyramidal cells. *Eur. J. Neurosci.* **12**, 781–792 (2000).
48. M. Fukaya, M. Uchigashima, S. Nomura, Y. Hasegawa, H. Kikuchi, M. Watanabe, Predominant expression of phospholipase Cbeta1 in telencephalic principal neurons and cerebellar interneurons, and its close association with related signaling molecules in somatodendritic neuronal elements. *Eur. J. Neurosci.* **28**, 1744–1759 (2008).
49. K. Matsuda, E. Miura, T. Miyazaki, W. Kakegawa, K. Emi, S. Narumi, Y. Fukazawa, A. Ito-Ishida, T. Kondo, R. Shigemoto, M. Watanabe, M. Yuzaki, Cbln1 is a ligand for an orphan glutamate receptor delta2, a bidirectional synapse organizer. *Science* **328**, 363–368 (2010).
50. Y. Kawamura, M. Fukaya, T. Maejima, T. Yoshida, E. Miura, M. Watanabe, T. Ohno-Shosaku, M. Kano, The CB1 cannabinoid receptor is the major cannabinoid receptor at excitatory presynaptic sites in the hippocampus and cerebellum. *J. Neurosci.* **26**, 2991–3001 (2006).

Acknowledgments: We thank the following for providing us with 4% PFA– and 9% glyoxal/8% acetic acid–fixed brain samples: A. Aiba at The University of Tokyo, K. Futai at University of Massachusetts Medical School, K. Nakamura at Primate Research Institute, Kyoto University, K. Sakimura at Niigata University, S. Tomita at Yale University, and M. Yuzaki at Keio University. **Funding:** This research was supported by the Japan Agency for Medical Research and Development (AMED) under the Brain Mapping by Integrated Neurotechnologies for Disease Studies (Brain/MINDS) project (grant no. JP17dm0207053h0004 to M.Y., JP14dm0207028h0003 to M.W.), and Grants-in-aid for Scientific Research from the Ministry of Education, Culture, Sports, Science and Technology of Japan (21 K06746 to K.K. and 20H03410 to M.Y., 22 K06784 to T.M., and 21H02589 to M.W.). **Author contributions:** Conceptualization: K.K. and M.W. Methodology: K.K., M.Y., and T.M. Investigation: K.K. and T.M. Visualization: K.K.. Supervision: M.W. Writing—original draft: M.W. Writing—Review and editing: K.K., M.Y., T.M., and M.W. **Competing interests:** The authors declare that they have no competing interests. **Data and materials availability:** All data needed to evaluate the conclusions in the paper are present in the paper and/or the Supplementary Materials.

Submitted 17 November 2022
Accepted 14 June 2023
Published 14 July 2023
10.1126/sciadv.adf7084